DETERMINISTIC ANALYSIS OF VANE-BLADE INTERACTIONS IN SELF-RECTIFYING RADIAL TURBINES FOR OWC PLANTS

J.M. Fernández Oro – B. Pereiras García – M. Galdo Vega

Energy Department. University of Oviedo
Politechnique School of Gijón. Campus de Viesques, EDZE. Gijón, Spain
jesusfo@uniovi.es; pereirasbruno@uniovi.es; galdomonica@uniovi.es

ABSTRACT

Self-rectifying turbines, providing unidirectional rotation for an alternating airflow, is an interesting impulse turbine for OWC plants. Despite of being penalized by its low maximum efficiency with respect to Wells turbines, it presents notable advantages that need to be explored with more knowledge of the flow pattern. For that purpose, a new set of simulations has been performed from a model previously developed and validated. The aim is to analyze the unsteady features of the flow and the rotor-stators interaction using a deterministic analysis. The simulations were developed in ANSYS FLUENT v12 and the results are presented in terms of turbulent kinetic energy and deterministic stresses. It is concluded that inner vanes (IV) of the turbine are identified as a critical contributor of generation of turbulence and unsteadiness in both outward and inward radial flows. Redesign of the IVs row is revealed necessary to improve the performance of the self-rectifying turbine.

NOMENCLATURE

C_A	Head Coefficient	Q	Flow rate
C_T	Torque coefficient	ΔP	Total pressure drop
ϕ	Flow coefficient	T	Torque
ω	Rotation speed	ρ	Air density
r_R	Mean radii of the turbine	b	Turbine width
U_R	Mean peripherical velocity		

INTRODUCTION

An Oscillating Water Column (OWC) is one of the most promising and most widespread systems for harnessing energy from waves. Wave energy power plants based on this concept convert wave energy into low-pressure pneumatic power. An OWC plant consists mainly of a submerged air chamber connected to the atmosphere through a duct where a turbine is installed. The successive sea water waves come into contact with the chamber, compressing and decompressing the air in it by the periodic motion of the oscillating sea water free surface. This periodic motion creates a bidirectional periodic flow through the turbine. Self-rectifying turbines are the best suited for working in such conditions because they can rotate in the same direction, independently of the flow direction. As a consequence of the especial flow conditions (variable load and two flow directions), a turbine design for wave energy conversion requires us to take into account a wide range of flow rates, not only the design point.

Different types of self-rectifying turbines have been proposed for use in OWC plants, the Wells turbine being the first one in 1976. The performance of the Wells turbine has been described in many articles and reports, (Raghunathan, 1995; Inoue, et al., 1986b). All the research agreed about the main disadvantages of this turbine: narrow range of flow rates with good efficiencies, poor starting characteristics, high speed operation, high noise level and high periodical axial thrust. In order to overcome the drawbacks of the Wells turbine certain modifications have been tested: self-pitch-controlled guide vanes (Kim, et al., 2001), variable-pitch angle blades, (Setoguchi, et al.,

OPEN ACCESS
Downloaded from www.euroturbo.eu

Copyright © by the Authors

2003), contra-rotating rotors (Raghunathan, et al., 1987; Gato, et al., 1996) or using different chord blades (Thakker, et al., 2007).

Another alternative proposed were the impulse turbines. They were suggested to overcome certain problem of the Wells turbine, in both axial and radial configurations. There are reports which compare the Wells and axial impulse turbines with fixed guide vanes. A comparison between turbine performances under irregular wave conditions is made in (Setoguchi, et al., 2006), and they show that axial impulse turbines are superior in running and starting characteristics under irregular flow conditions.

However, the interest of the present work is focused on the radial impulse turbine, proposed by (McCormick, et al., 1992). This turbine (**Figure 1**) is equipped with a rotor, and two rows of guide vanes, inner (IV) and outer (OV). In (Setoguchi, et al., 2002) an experimental work of the impulse radial turbine was made; it shows that this kind of turbine has an acceptable efficiency without a bidirectional axial trust. The main advantages of the radial turbine are its low manufacturing cost, its ruggedness and the high specific energy obtained due to the radial configuration (Dixon, 2005), although the turbine causes a high damping which on the OWC and it is penalized by the low maximum efficiency (Setoguchi, et al., 2006).

In order to develop a high performance radial turbine, in (Takao, et al., 2005) a turbine with pitch-controlled guide vanes was proposed, which in terms of efficiency is better, but its manufacturing and maintenance is quite expensive. More recent works show that redesigning the blade and vanes geometry leads the mean efficiency of the turbine to be increased up to a 5% (Pereiras, et al., 2011)

The authors consider that the radial impulse turbine could have potential for further improvements. Nowadays, there are not studies about the flow pattern inside the radial impulse turbine except for the one previously cited (Pereiras, et al., 2011). The aim of this work is to go deeper in the knowledge of the flow patterns, putting the focus on the flow unsteadiness and secondary flows. In the present paper, a 3D CFD model, previously validated (Pereiras, et al., 2011), was resolved using the FLUENT software and the results have been used as the numerical database for further numerical, deterministic post-processing.

In this case, rotor-stator interaction, in both direct and inverse flow direction, is a key factor conditioning the aerodynamic performance of the stage and justifies the use of the deterministic framework to analyze in detail the origin and nature of the unsteadiness. It allows a physical comprehension of the complexity, three-dimensionality and unsteadiness of the flow structures in the interaction regions of the turbine. In this context, the evaluation of the non-uniformities induced by the vanes over the blade-to-blade distributions is presented and fluctuation levels in the blade loadings, derived from deterministic non-uniformities, are provided in the relative frame of reference. The comparison between direct and reverse modes is definitive to understand the aerodynamic performance of the turbine and advances regions of generation of noise sources which can be correlated to noise emission levels in the propagation region.

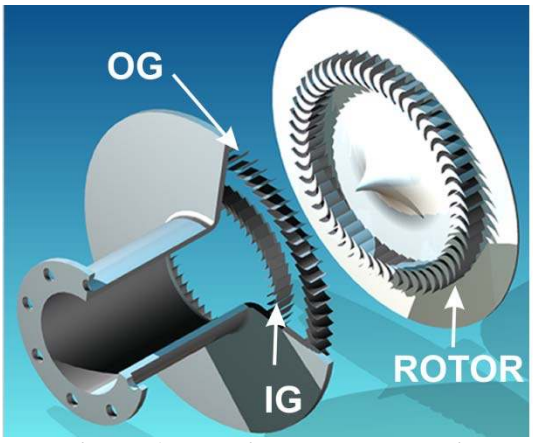

Figure 1a. Radial Impulse Turbine.

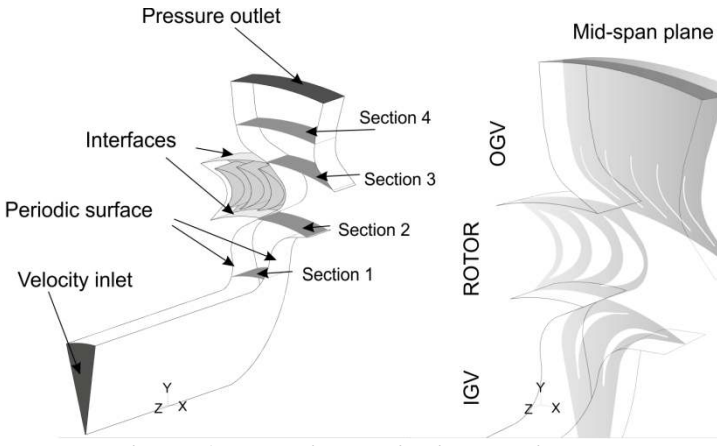

Figure 1b. Turbine periodic domains.

NUMERICAL MODEL

The flow simulation is solved with ANSYS FLUENT v12®. Since the computational volume includes rotating components (ω = 234 rpm), the sliding mesh technique is used in order to manage the relative movement between the rotor and the stator of the turbine. A hexaedrical unstructured grid of 500.000 cells is built in Gambit with special refinement towards solid contours.

The flow model solves the incompressible fluid conservation equations by using a segregated solver. The realizable k-ε turbulence model was used with the standard wall function. The time dependent term is approximated with a second order implicit scheme. The pressure-velocity coupling was recreated through the SIMPLE (Semi-Implicit Method for Pressure Linked Equations) algorithm. The highest order MUSCL (Monotonic Upstream-Centered Scheme for Conservation Laws) scheme has been used for convection terms discretization and the classical central differences approximations for diffusion terms. In order to reduce variable storage and to improve numerical accuracy, we have reduced the 3D calculation domain to a small angular sector with periodic boundaries. Additional boundaries, like inlet velocities and pressure outlets, are depicted in Figure 1. A tip clearance of 2.2% of the span was also introduced in the model. Details of the blade and guide vanes geometry can be consulted in (Pereiras, et al., 2011).

Since the time scales of the wave motion (alternatively unsteady) are much longer than those related to the flow phenomena within the turbine stage, it has been assumed that the turbine works in steady flow conditions, rotating unsteadily. Turbine performance (Figure 2) under steady flow conditions was evaluated in terms of the classical dimensionless coefficients of bidirectional turbines: C_A, C_T, ϕ, which are the head, torque and flow coefficient respectively. The definition of the coefficients is as follows:

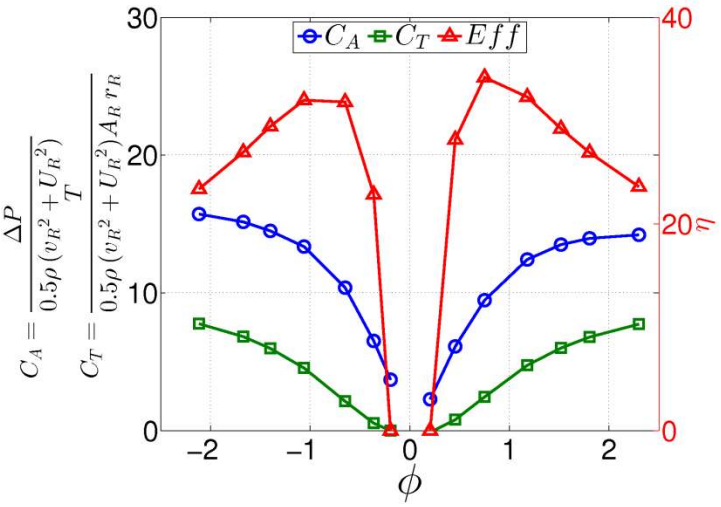

Figure 2. Dimensionless performance of the turbine.

DETERMINISTIC ANALYSIS

Time-averaged flow. The time-averaged flow provides an initial picture of the flow patterns within the turbine. In particular, this time-mean footprint of the unsteady structures is analyzed for both outward and inward radial flows and for different operating conditions: low (ϕ=±0.45), nominal (considered as maximum efficiency, ϕ=±0.75) and high (ϕ=±1.10) flow rates.

Figure 3 shows the averaged radial velocity in the midspan section of the turbine in a typical blade-to-blade representation. It has been made non-dimensional with a characteristic throughflow velocity defined for every case as $\bar{\bar{v}}_R = Q/2\pi r_R b$, where r_R is the mid-radius of the rotor blades and b is the span. Note that both fixed and rotating reference frames are included in the figure, through an image composition of the different domains. In the rotor frame, the averaged flow has been computed in the relative frame (periodic after 93 time steps), whereas IVs and OVs domains have been calculated in the absolute frame (periodic after 31 time steps).

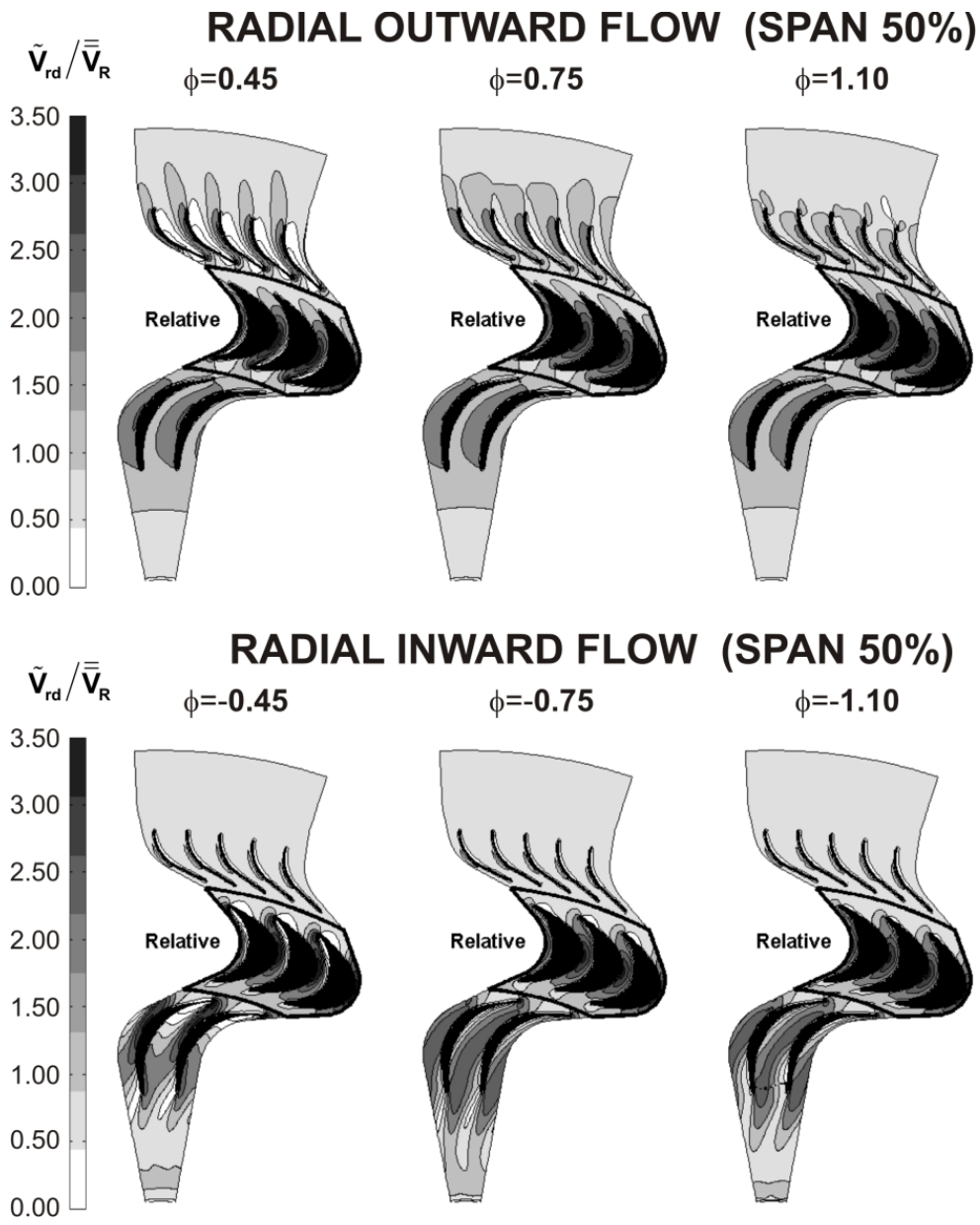

Figure 3. Time-averaged radial velocity at midspan for outward and inward radial flows.

Basically, the figure reveals that major losses are clearly developed in the outlet fixed vanes (the outer vanes in the case of the radial outward flow –maps on top- and the inner vanes in the case of the inward radial flow –maps on bottom-), being more important with high flow rates. Another significant feature is the negative incidence at the leading edge of the rotor blades for low flow rates (observe the white region of detached flow in the pressure side of the blades, mainly for $\phi=\pm0.45$), which provokes a drastic flow separation within the rotor passages. Finally, note also how the rotor blades are influencing the outlet wakes in the case of inward flow (they are tilted downstream), for all the flow rates analyzed.

In order to discuss other flow distributions out-of-midplane, four different transversal sections (planes 01 to 04, see Figure 1.b) have been defined to study the spanwise distribution of the flow. Figure 4 shows in detail the non-dimensional radial velocity in sectors 03 (rotor outlet) and 04 (OV's exit) for all the flow rates considered in case of outward radial flow. In sector 03, the blockage effect of the five OVs is the main flow pattern observed for all the flow rates. Moreover, it is the only feature noticeable for the nominal conditions. At $\phi=1.10$, it is revealed the effect of the

interaction between the wake flow of the IVs and the tip vortex of the rotor blades over the inlet flow of the OVs (two white "hot spots"). However, at ϕ=0.45, the mechanism that is convected downstream is the interaction of the rotor inlet flow separation with the wake flow of the inner vanes, whose combination with the blocked flow of the OVs is revealed here (less intense in the tip region). Because the tip vortex interaction at high flow rates is more intense, the effect is also tangentially shifted at the rotor exit with respect to the separated flow.

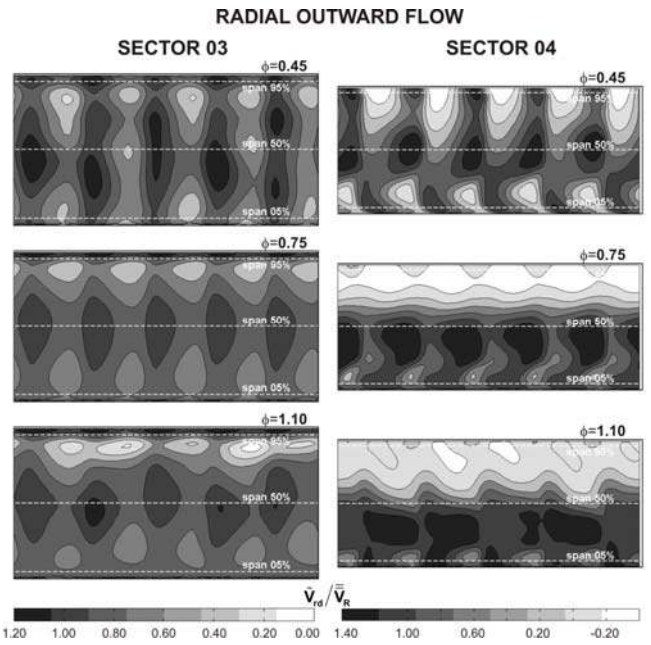

Figure 4. Time-averaged radial velocity at transversal planes 3 and 4 (outward flow).

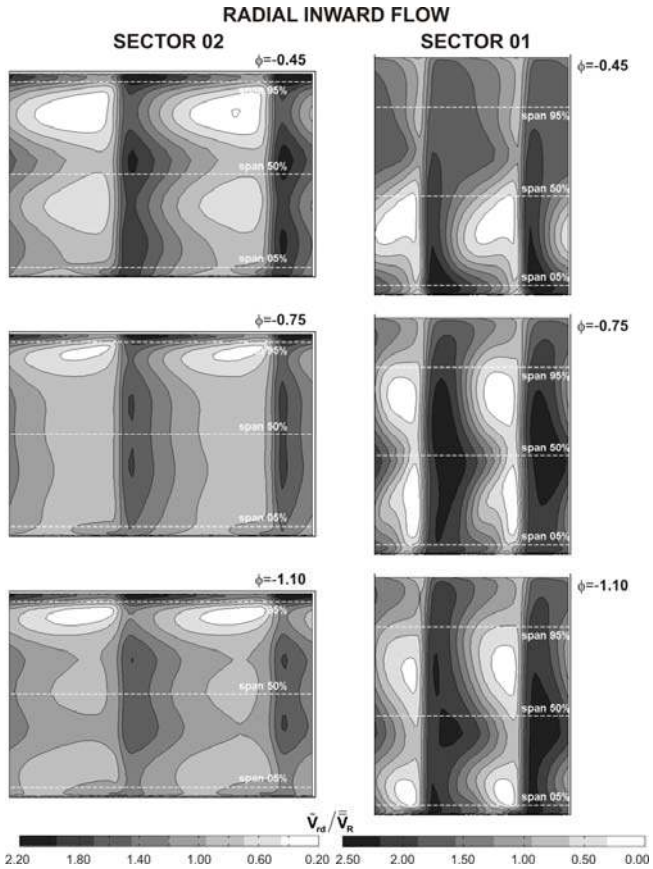

Figure 5. Time-averaged radial velocity at transversal planes 2 and 1 (inward flow).

On the other hand, sector 04 illustrates the tip vortex of the OVs (in the hub region). In this case, the interactions due to the flow separation at low flow rates are completely mixed out whereas rotor vortex interactions at high flow rates are still present. Note that at nominal conditions, the averaged effect of the rotor tip vortex is already noticeable in the tip region (95% span). Large areas of reverse flow are also visible in the tip region at the outlet.

Finally, Figure 5 completes the description of the time-averaged flow with the representation of the inward flow at sector 02 (IVs inlet in inward mode) and sector 01 (turbine outlet in inward mode). As expected, the IVs blockage is the more relevant characteristic. Here, there is no effect of the 5 OVs on the flow structures (OVs are too thin to provoke relevant non-uniformities or further interaction). It is also observed more detached flow at low flow rates, more intense at the tip region due to a higher interaction with the incoming tip vortex of the rotor blades.

In sector 01 there is also a massive detached flow in the IVs downstream. At low flow rate, there is a region between 50 and 5% span with a low radial velocity provoked by the detached flow of the IVs. Conversely, at nominal and high flow rates, a double structure is now developed; between 95 and 50% span, a low radial velocity is further evolved into detached flow, whereas between 50 and 5% span, it is the own effect of the vortex of the IVs the more significant flow pattern.

Turbulent and Deterministic Kinetic Energy. Deterministic stresses account for the time-averaged contribution of the unsteady sources of the flow over the averaged flow patterns. The comparison of those terms with the turbulent (Reynolds) stresses provides a comprehensive picture of the energy fluxes taken place within the turbomachinery stages. This section is devoted to compare them in both blade-to-blade planes and transversal sectors to highlight the distributions of unsteady sources and turbulent spots for both outward and inward radial flows.

Turbulent (TKE) and deterministic (DKE) kinetic energies, defined as the sum of the main diagonal of the stress tensors, have been considered here as representative variables for a more compact analysis. TKE reveals the zones of generation of turbulence providing an averaged level of velocity fluctuations due to turbulent mechanisms, while DKE reveals those zones with large velocity fluctuations due to the periodic interaction of moving and fixed surfaces. Additionally, it was necessary to time-average the unsteady distributions of TKE to compare them accordingly. These variables have been also non-dimensionalized using a typical rotor blade peripheral velocity, $U_R = \omega r_R$. Note that the rotor domain has been also represented in the relative frame in a similar fashion to previous Figure 3.

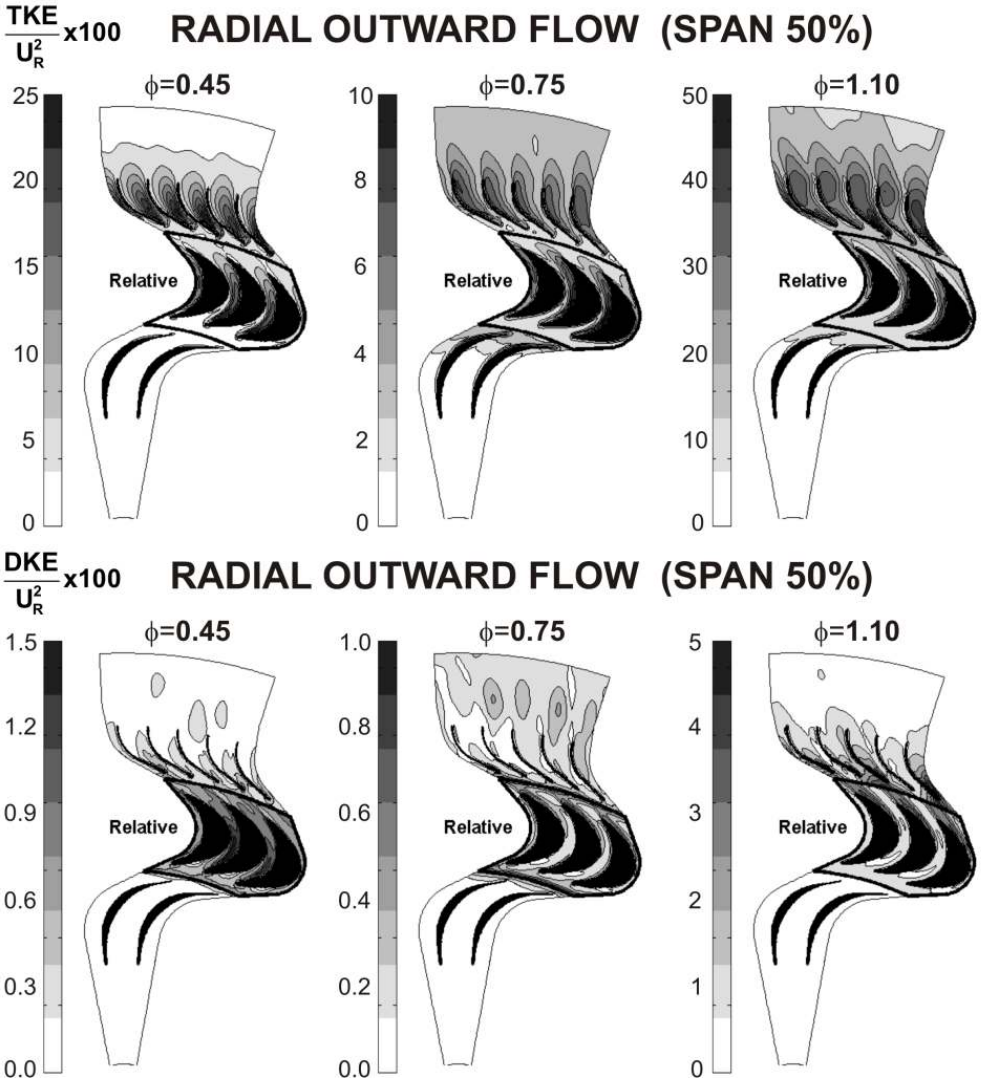

Figure 6. Time-averaged TKE and DKE at midspan for outward radial flow.

Figure 6 (on top) shows the averaged TKE at midspan for outward flow. At ϕ=0.45, high levels of turbulence are observed within the rotor passages due to the massive incidence losses. These losses are progressively reduced with increasing flow rates. Concerning the OVs, it is observed that they are never working properly for the whole range of operating conditions, especially at high flow

rates. Note also the appearance of hot spots in the outer vanes due to clocking effects with the inner vanes (once again at ϕ=1.10).

Deterministic Kinetic Energy (on bottom) shows similar trends with inner guide vanes completely free of unsteady sources, and major interaction in the interrow region of blades and OVs at high flow rate, also participating of clocking mechanisms.

To complete the picture of the outward flow, Figures 7 and 8 show TKE and DKE distributions respectively in the transversal sectors at the outlet of the stage. In particular, the averaged TKE distributions at sector 03 show the impact of the inner guide vanes; in particular the generation and shedding of turbulent structures at high flow rates. Additionally, sector 04 presents the turbulent wakes developed at the turbine discharge. There is an evident lack of periodicity between consecutive vanes thus suggesting the relevant interaction of the wake flow of the IVs. It is also remarkable the different spanwise lean of the OVs wakes depending on the operating conditions. Note also the dramatic levels of turbulence at ϕ=1.10.

Deterministic kinetic energy shows less disorder in the case of nominal conditions at sector 03. There is a reinforcement of unsteadiness due to the interaction with the inner guide vanes (see case ϕ=0.45), which is shifted in the case of ϕ=1.10. This pattern is similar to that one described in the case of the time-averaged structures of the radial velocity. Finally, sector 04 reveals two hot spots of fluctuation in the tip region induced by the clocking with the inner guide vanes (at low flow rate). In the hub, the fluctuation of the vane's tip vortex is the more relevant pattern at high flow rates.

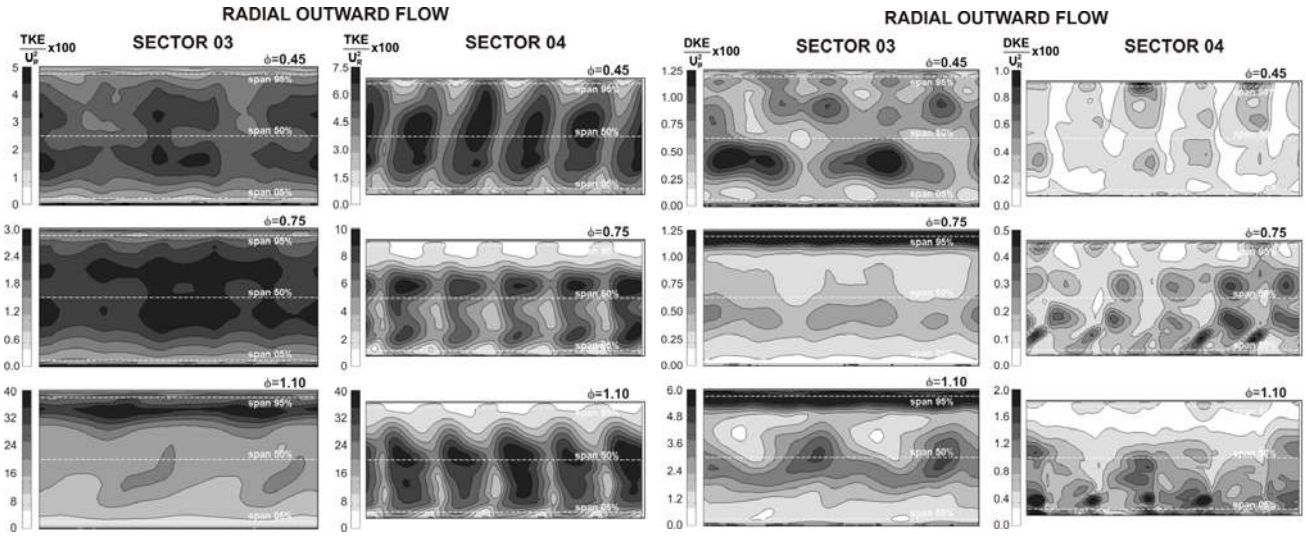

Figure 7. Time-averaged TKE at transversal planes 3 and 4 (outward flow).

Figure 8. Time-averaged DKE at transversal planes 3 and 4 (outward flow).

Similar analysis is assessed now for the inward flow in Figures 9 to 11. Firstly, blade-to-blade distributions of TKE and DKE are presented in Figure 9. On top, there are new evidences of poor guidance at the rotor inlet in the case of low flow rate, which are progressively corrected as the throughflow radial velocity is increased. Flow separation and turbulence generation is clearly visible at the leading edge of the inner vanes. As the flow rate is increased, this separation is concentrated towards the vane, unblocking the vanes passages. However, at high flow rates, the turbulence levels are extremely high. In the case of the DKE (bottom maps), there is an evident arising of unsteadiness in the suction side of the vanes, close to their trailing edges. This is a consequence of the interaction that the rotor blades are producing over the separated flow in the vane wakes at nominal and high flow rates.

In sector 02 of Figure 10, the results show a quite uniform flow, with only generation of turbulence associated to the stagnation conditions of the inner vanes. At high flow rates, there is a better rotor guidance, less incidence losses (the spanwise band of turbulence is reduced) but major

tip vortex from the rotor, thus leading to a clear peak of high turbulence concentrated in the tip regions of the higher flow rate. In sector 01, turbulence maps present very different structures according to the flow rate under operation. At low flow rates, the previous turbulence bands observed in sector 02 are broadened, covering almost the whole transversal area. At nominal conditions, it presents the maximum values close to the tip, whereas at high flow rate, the maximum turbulence is concentrated towards the center of the passage.

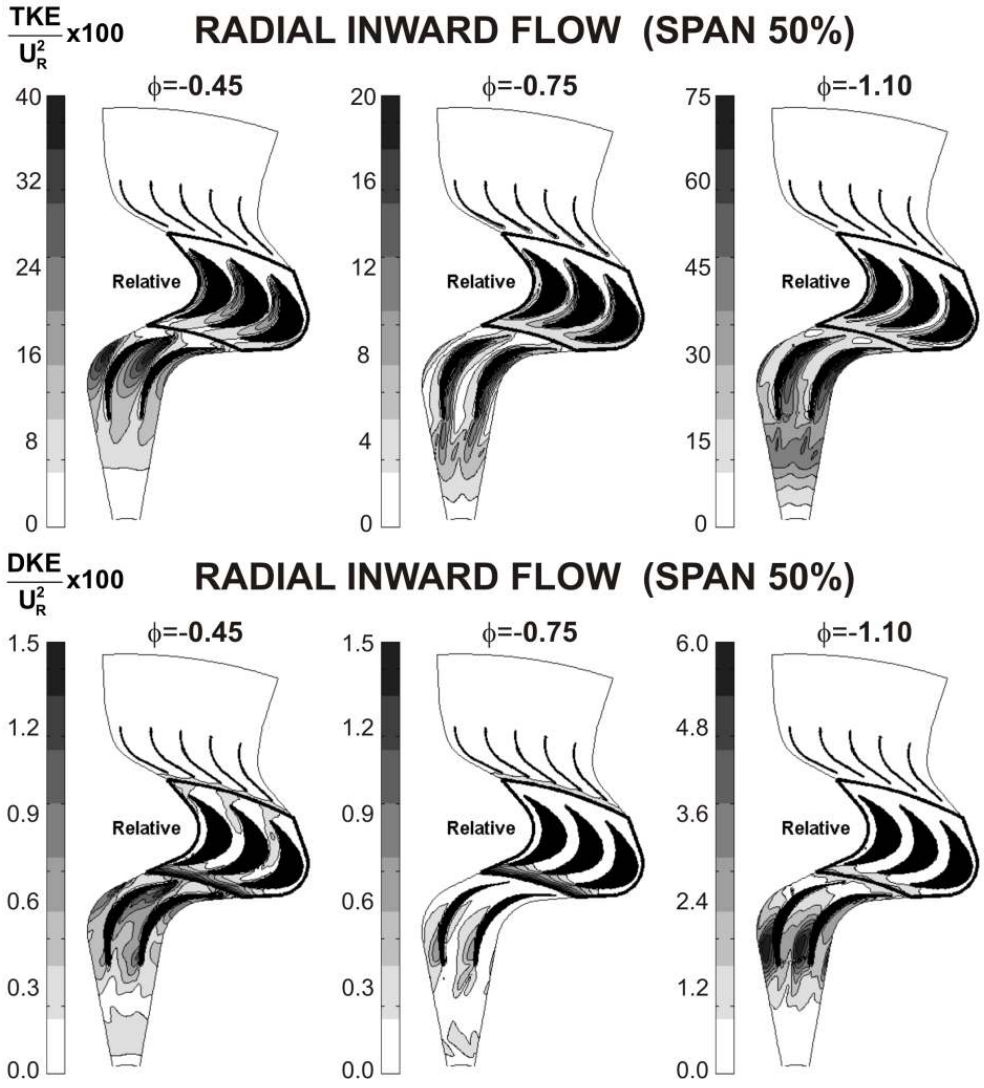

Figure 9. Time-averaged TKE and DKE at midspan for inward radial flow.

Following, Figure 11 reveals those regions with unsteady fluctuations in the sectors upstream and downstream of the inner vanes. Sector 02 appears as a calm region, and only fluctuation in the tip of the vanes is observed. This intensification must be provoked by the periodic passing of the rotor wakes inducing an oscillation of the stagnation conditions. At the IVs outlet (sector 01), there is a notable disorder of the unsteadiness, with areas of maximum values that are displaced as a function of the flow rate.

Additional insight is addressed if blade-to-blade maps of TKE and DKE in both outward and inward radial flows (Figures 6 and 9) are pitch-averaged. This is presented in Figure 12, where it is showed the radial evolution of these variables with the throughflow. In the case of outward flow (plots on the left), there is a progressive increase in both TKE and DKE along the turbine 1 1/2 stage. Turbulence is increased along the different rows, partially reducing its intensity in the interrow gaps. On the contrary, deterministic energy is always peaked in the gap zones between the

rows. Maximum turbulence is developed at the trailing edge of the OVs, while maximum unsteadiness is observed at leading edge of the OVs. Note also that turbulence levels are almost one order of magnitude higher than deterministic ones. Finally, notice the excessive values found in the case of high flow rate.

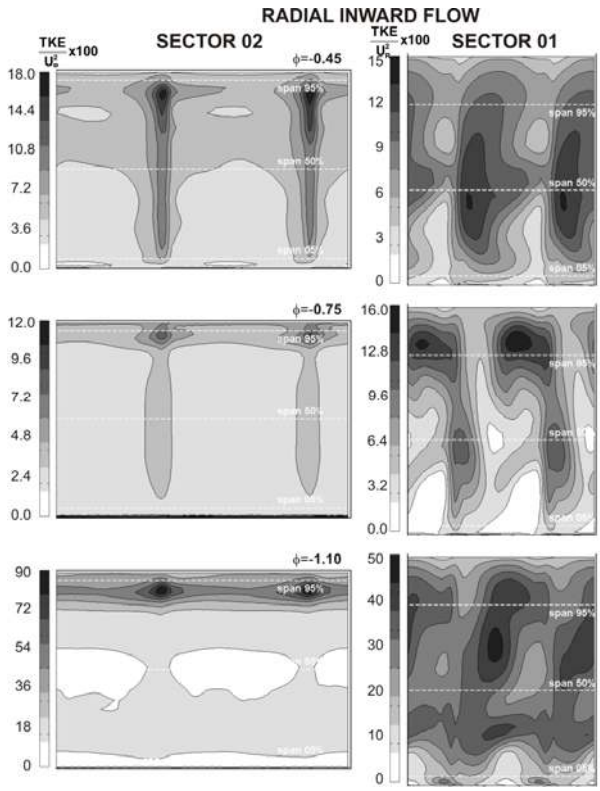

Figure 10. Time-averaged TKE at transversal planes 2 and 1 (inward flow).

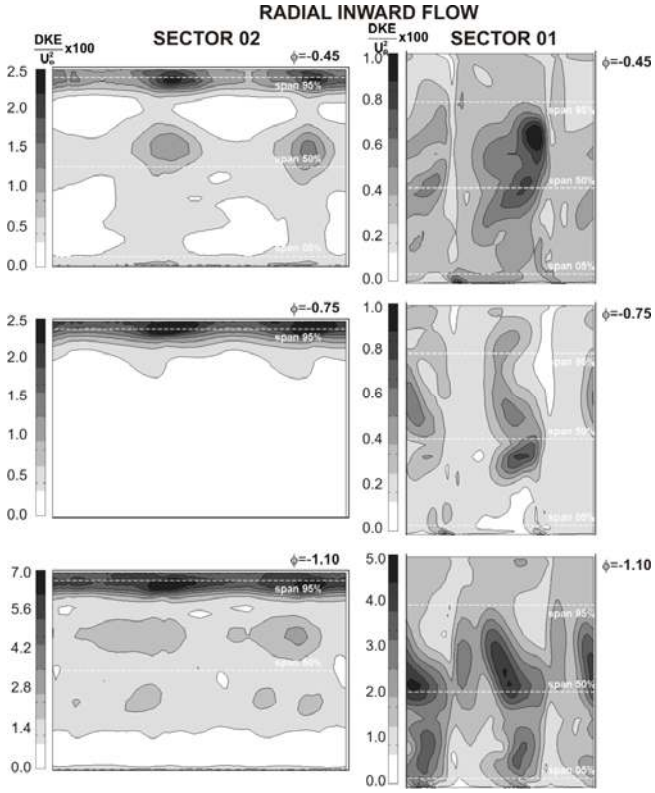

Figure 11. Time-averaged DKE at transversal planes 2 and 1 (inward flow).

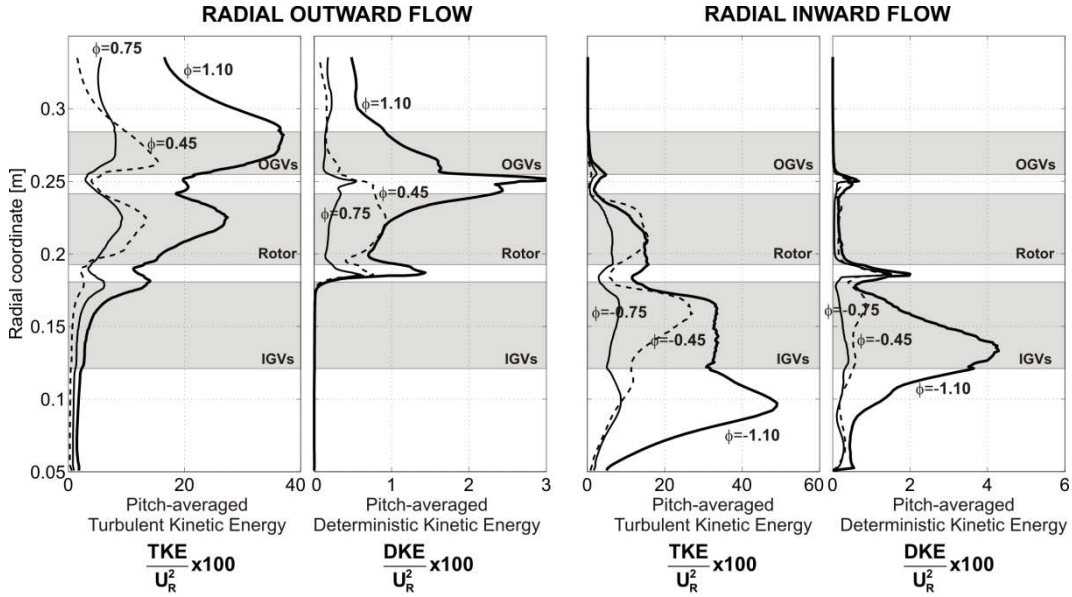

Figure 12. Throughflow distributions of pitch-averaged TKE and DKE for both outward and inward radial flows.

On the other hand, the inward flow presents also an increasing rise of TKE and DKE along the streamwise direction. As before, local minima of turbulence are observed in the gap regions, which are associated to local maxima of deterministic unsteadiness in the interrows. Note again that maximum turbulence is found downstream the inner vanes (at ϕ=-1.10) whereas maximum deterministic energy is observed at their trailing edges.

Deterministic decomposition. The unsteady flow in any turbomachine can be further decomposed in four different components using a set of averaging operators that include time-averaging (in both reference frames) and pitch-averaging. As a consequence, the throughflow, the blade-to-blade fluctuations and the vane-to-vane non-uniformities in the whole domain can be recovered from the unsteady flow. Finally, subtracting all these averaged distributions from the original time evolution of the velocity maps, a pure unsteady interaction component is also identified.

This procedure, valid for single rotor-stator stages, can be also employed here because both fixed rows (IVs and OVs) have been modelled with the same tangential periodicity. Additionally, interpolation and relocation routines are necessary to translate the original data associated to the body-fitted mesh employed in the Fluent code into a structured grid in the Matlab post-processing (in both blade-to-blade and transversal planes). This procedure allows a tangential shift of the dataset over time, so subtraction of the different averaged maps obtained in both absolute and relative frames is possible. More details of this post-processing can be found in (Fernández Oro et al., 2013) for a similar centrifugal geometry in a small squirrel-cage fan.

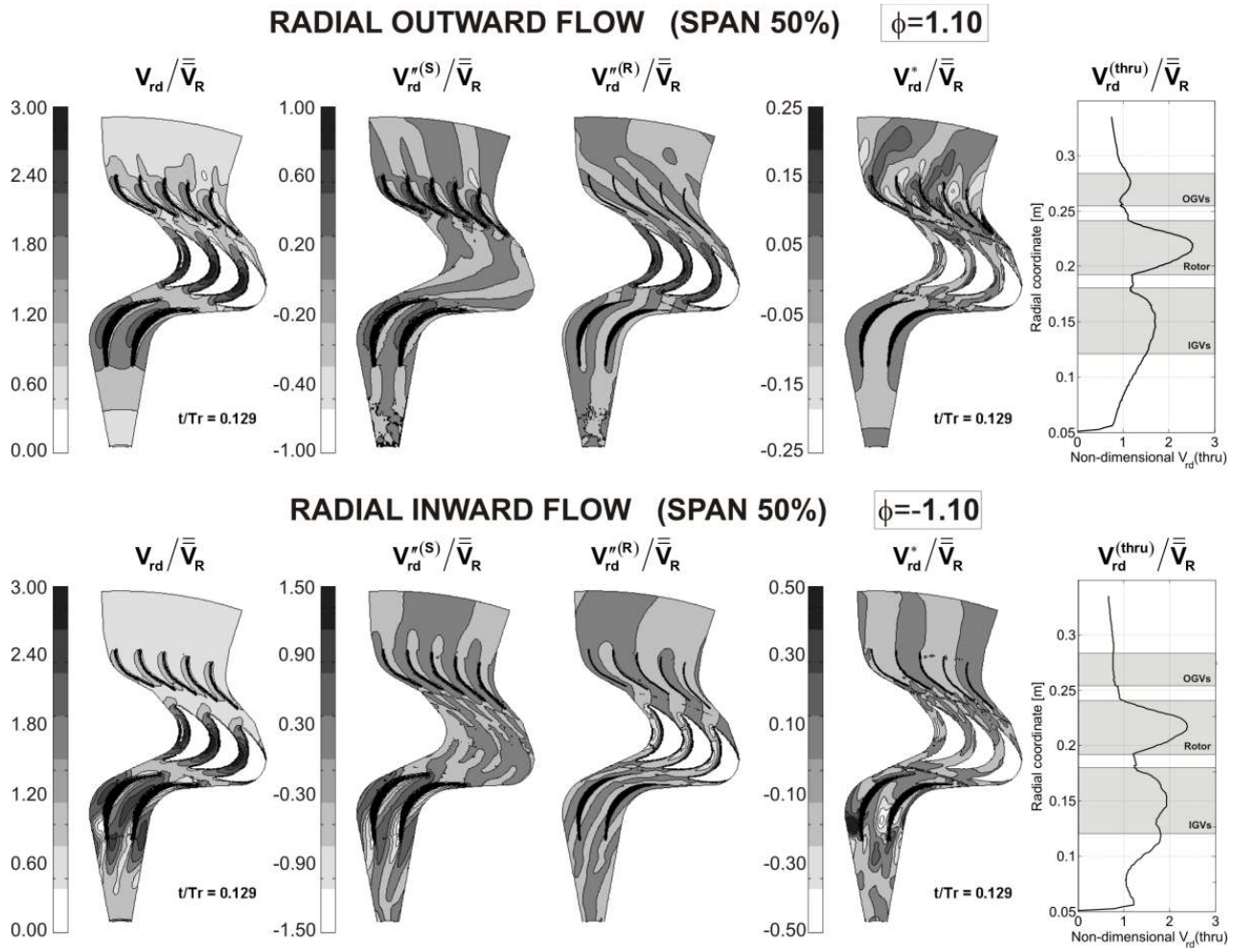

Figure 13. Deterministic decomposition of radial velocity at midspan for both outward and inward radial flows at high flow rate.

Figure 13 shows the decomposition of the unsteady flow of the non-dimensional radial velocity in the case of high flow rate for both outward (top) and inward (bottom) radial flow. The unsteady flow shown here is a single snapshot in a particular instant, whereas both fixed (V_{rd}"(S)) and rotating ((V_{rd}"(R)) averaged non-uniformities are steady maps. The throughflow distribution (plot on the right) shows the radial evolution of the velocity, significantly increased within the rotor passages. In the case of the fixed reference (second map from the left), the non-uniformities coming from the IVs are clearly visible and convected downstream through the stage. Note also their interaction with the wake flow of the OVs leading to the appearance of hot spots due to clocking. Similarly, in the relative frame (second map from the right) the rotor wakes, identified as the basic mechanism of non-uniformity, are perfectly aligned with the rotor trailing edge. Finally, the remaining map shows the unsteady pure interaction between moving and fixed domains at that particular snapshot. Regions of positive and negative fluctuation are generated within the rotor passages interacting with the IVs and convected downstream onto the outlet vanes. In the gap between the rotor and the OVs, these fluctuations are reinforced and new areas with high interaction are established within the vane surfaces and even downstream, at the turbine exit. Two outcoming large wakes show again the influence of the IVs on the interaction patterns.

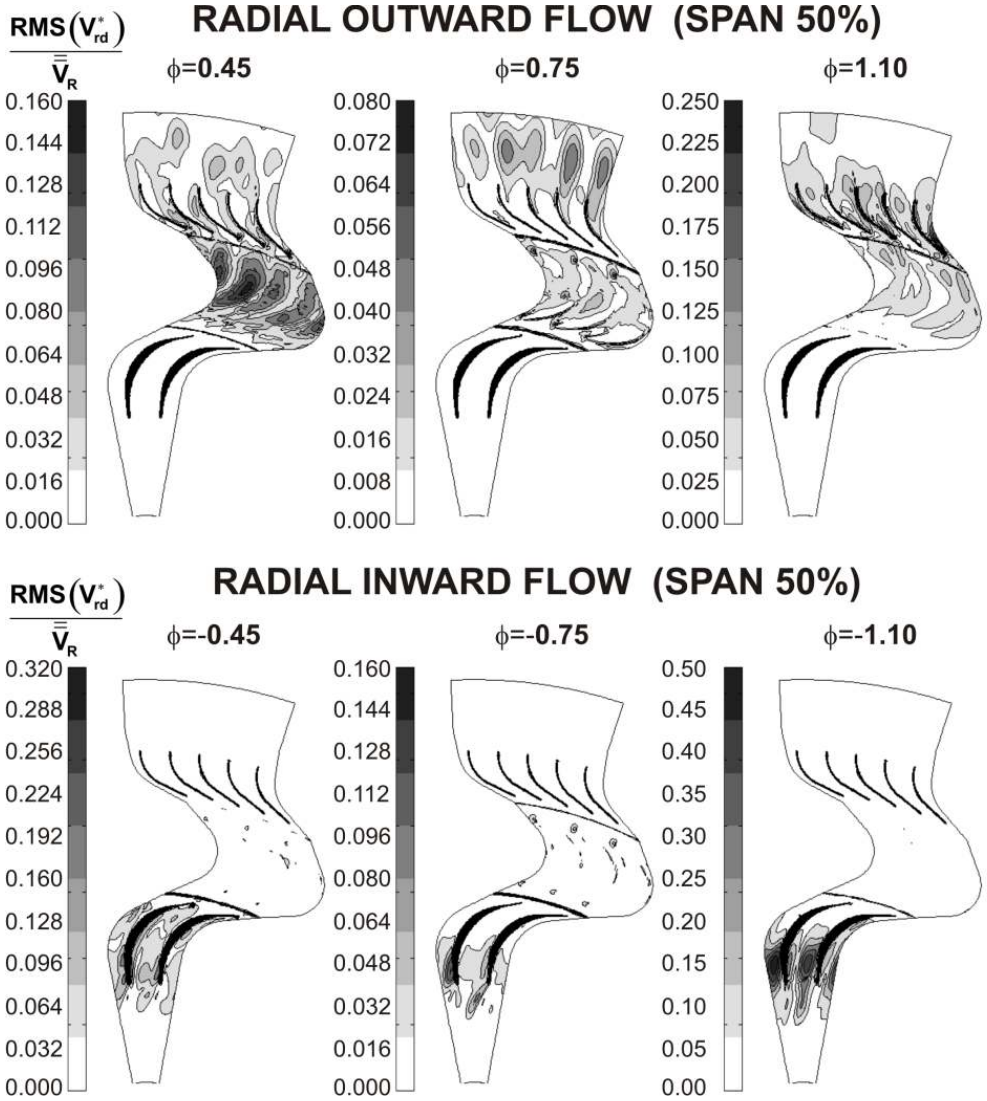

Figure 14. RMS distributions of pure unsteadiness for outward and inward radial flows.

Inward flow at high flow rate (Figure 13, bottom) illustrates a similar decomposition. In this case, the non-uniformities of the OVs are less important and they are rapidly diffused within the rotor passages (see the fixed non-uniformities in the second map on the left). The rotor wakes are evident again in the representations of the blade-to-blade non-uniformities, being stretched and realigned with the inner passage due to the severe reduction of the cross-sectional area. This provokes also three-dimensionality and spanwise displacement of the secondary flows observed in previous sector 01. Concerning the pure unsteady component, major interaction is revealed over the detached flow of the suction side in the vanes, due to the periodic passing of rotor wakes changing the angle of the incident flow.

To conclude the analysis, Figure 14 presents the pure unsteady component for all the cases analyzed in the paper. The RMS value of the pure interaction has been calculated so the unsteady distributions are reduced into a single map, where high interaction regions are highlighted in these new representations. As expected, major interaction is observed in the case of outward flow. At low flow rates, flow separation in the rotor blades is unstable and a significant contributor to total unsteadiness. All the cases present important unsteadiness in the OV domain, especially at high flow rates with hot spots over the outer vanes induced by the IVs. In the case of the inward flow, only high unsteadiness is observed in the vicinity of the IVs, being significantly intense at high flow rates.

CONCLUSIONS

This paper presents the application of a numerical methodology to address the impact of unsteadiness in a self-rectifying radial turbine. Deterministic correlations have been employed to perform the analysis in both blade-to-blade and transversal planes, focusing on the differences in the vane-blade interaction depending on the flow direction (outward and inward flow) and as a function of the flow rate.

In the case of outward flow, it has been observed at midspan that the IV rows generates a large amount of unsteadiness rotor downstream, due to the important non-uniformity associated to its wake flow which is transported downstream onto the OVs. Hot spots of interaction have been identified over the pressure sides of the outer vanes, which position is conditioned by the clocking mechanisms of the inlet vanes. On the contrary, for inward flow, the non-uniformity of the OVs is very weak, so there is no relevant impact on the downstream rows. However, the interaction of the periodic rotor wakes on the detached conditions in the suction sides of the inner vanes is dramatic. It is revealed that high flow rates exhibit a clear unsteadiness at the IVs, as a consequence of the jet-wake pattern induced by the blades, which generates a pulsation in the separation region.

Additionally, the results in the transversal planes have illustrated the relevant presence of tip vortices in the all the rows of the turbine. Both OVs and IVs exhibit intense tip vortices at large low rates, in case of outward and inward flow respectively. Moreover, the higher radial velocity at the IVs for inward conditions, as well as the reduced size of the discharge area, lead to major unsteadiness and a significant increase of secondary flows at the stage exit for inward flow. Only the effect of the tip vortex of the rotor blades seems to have an impact in the unsteady conditions of the OVs in the case of outward flow for high flow rates.

Pitch-averaged distributions of TKE and DKE have highlighted that the turbine is not working efficiently at high flow rates, being particularly evident in the case of inward flow. In that case, major interaction and generation of turbulence is observed at the IVs of the stage. For radial outward flow, though unsteadiness and turbulence at IVs are quite calm, the non-uniformity introduced by the IVs induces flow disorder downstream, leading to the appearance of hot spots, unsteadiness and high turbulence due to incidence losses at off-design flow rates.

Consequently, the deterministic analysis has allowed the identification of the IVs as a critical contributor of generation of turbulence and unsteadiness in both outward and inward radial flows. Redesign of the IVs row is revealed necessary to improve the performance of the self-rectifying

turbine, and inlet non-uniformities have been demonstrated to cause an especial detrimental effect on the downstream flow structures.

REFERENCES

Dixon S. L. Fluid mechanics and thermodynamics of turbo machinery [Book]. - [s.l.] : BUTTERWORTH-HEINEMANN, 2005. - 5. - ISBN: 978-0-7506-7870-4.

Fernández Oro, J.M. [et al.] Numerical methodology for the assessment of relative and absolute deterministic flow structures in the analysis of impeller–tongue interactions for centrifugal fans [Journal] // Computers and Fluids. - 2013 - Vol. 86. - pp. 310-325.

Gato L.M.C. and Curran R. Performance of the Biplane Wells Turbine [Journal] // Journal of Offshore Mechanics and Arctic Engineering (OMAE). - 1996. - Vol. 118. - pp. 210-215.

Inoue M. [et al.] Simulation of Starting Characteristics of the Wells Turbine [Conference] // ASME 4th Fluids Mechanincs, Plasma Dynamics and Lasers Conference. - Atlanta : [s.n.], 1986b. - AIAA-86-1122.

Kim T.H., Setoguchi T. and Kaneko K. The optimization of blade pitch settings of an air turbine using self-pitch-controlled blades for wave power conversion [Journal] // Journal of Solar Engineering. - 2001. - Vol. 123. - pp. 382-386.

McCormick M.E., Rehak J.G. and Williams B.D. An Experimental Study of a Bidirectional Radial Turbine for Pneumatic Wave Energy Conversion [Journal] // Mastering the Oceans Through Tecnology. - 1992. - Vol. Vol. 2. - pp. 866-870.

Pereiras B. [et al.] An Improved Radial Impulse Turbine for OWC [Journal] // Renewable Energy. - 2011. - 5 : Vol. 36. - pp. 1477-1484.

Pereiras B. [et al.] Tip Clearance Effect on the FLow Pattern of a Radial Impulse Turbine for Wave Energy Conversion [Journal] // Journal of Turbomachinery - Transactions of the ASME. - [s.l.] : ASME, 2011. - 4 : Vol. 133.

Raghunathan S. [et al.] The Biplane Wells Turbine [Conference] // Proceedings of the OMAE conference. - Houston : [s.n.], 1987. - pp. 475-479.

Raghunathan S. The Wells Turbine for Wave Energy Conversion [Journal] // Prog. Aerospace Sci. - 1995. - Vol. 31. - pp. 335-386.

Setoguchi T. [et al.] A Modified Wells Turbine for Wave Energy Conversion [Journal] // Renewable Energy. - 2003. - Vol. 28. - pp. 79-91.

Setoguchi T. [et al.] A Performance Study of a Radial Impulse Turbine for Wave Energy Conversion [Journal] // Journal of of Power and Energy. - 2002. - Vol. 216 (A1). - pp. 15-22.

Setoguchi T. and Takao M. Current Status of Self Rectifying Air Turbines for Wave Energy Conversion [Journal] // Energy Conversion and Management. - 2006. - 46. - pp. 2382-2396.

Takao M., Fujioka Y. and Setoguchi T. Effect of Pitch-Controlled Guide Vanes on the Performance of a Radial Turbine for Wave Energy Conversion [Journal] // Ocean Ingenieering. - 2005. - 32. - pp. 2079-2087.

Thakker A. and Abdulhadi R. Effect of Blade Profile on the Performance of Wells Turbine under Unidirectional Sinusoidal and Real Sea Flow Conditions [Journal] // International Journal of Rotating Machinery. - 2007. - doi:10.1155/2007/51598.